

# Quantification of forward scattering based on the analysis of double-pass images in the frequency domain

Joan A. Martínez-Roda,<sup>1</sup>  Carlos E. García-Guerra,<sup>1</sup> Fernando Diaz-Doutón,<sup>1</sup> Jaume Pujol,<sup>1</sup> Antoni Salvador<sup>2</sup> and Meritxell Vilaseca<sup>1</sup>

<sup>1</sup>Centre for Sensors, Instruments and Systems Development (CD6), Universitat Politècnica de Catalunya (UPC), Terrassa, Spain

<sup>2</sup>Ophthalmology Service, Hospital Universitari Mútua de Terrassa, Terrassa, Spain

## ABSTRACT.

**Purpose:** To assess forward intraocular scattering by means of a new parameter (Frequency Scatter Index, FSI<sub>3</sub>) based on the analysing double-pass retinal images in the frequency domain, which minimizes the impact of aberrations on the results.

**Methods:** A prospective observational study was carried out in the Department of Ophthalmology, Hospital Universitari Mútua de Terrassa (Spain) on a group of 19 patients diagnosed with nuclear cataracts of various LOCSIII grades and a control group (CG) with nine healthy eyes. We recorded double-pass retinal images with a custom set-up based on a high-sensitivity digital camera. The FSI<sub>3</sub> was then computed using spatial frequencies below three cycles per degree. A preliminary validation of the FSI<sub>3</sub> was performed on an artificial eye and two eyes of volunteers with and without commercial diffusers, and under defocus.

**Results:** The FSI<sub>3</sub> was hardly affected by defocus values up to 2.50 D. The mean (and standard deviation) FSI<sub>3</sub> values were as follows: for the CG, 1.19 (0.21); and for LOCSIII grades nuclear opacity 1, 2 and 3, 1.30 (0.12), 1.62 (0.21) and 1.85 (0.21), respectively. Eyes with cataracts showed FSI<sub>3</sub> values significantly different than healthy eyes ( $p = 0.001$ ). A good correlation ( $\rho = 0.861$ ,  $p < 0.001$ ) was found between the FSI<sub>3</sub> and objective scatter index provided by a commercial instrument.

**Conclusion:** Since aberrations have little impact on the FSI<sub>3</sub>, the light scatter assessment becomes less dependent on the patient's refractive error compensation and the presence of higher-order aberrations. The FSI<sub>3</sub> can further the clinical and scientific understanding of forward intraocular scattering.

**Key words:** aberrations – cataracts – double-pass – forward intraocular scattering

The copyright line for this article was changed on 17 September 2019 after original online publication.

Acta Ophthalmol. 2019; 97: e1019–e1026

© 2019 The Authors. Acta Ophthalmologica published by John Wiley & Sons Ltd on behalf of Acta Ophthalmologica Scandinavica Foundation.

This is an open access article under the terms of the Creative Commons Attribution License, which permits use, distribution and reproduction in any medium, provided the original work is properly cited.

doi: 10.1111/aos.14122

## Introduction

Forward intraocular scattering is a phenomenon of human vision that can currently be quantified by psychophysical

and objective methods (Westheimer & Liang 1994; Franssen et al. 2006). When commercial devices have been used to compare both types of methods in patients with posterior capsule

opacification (Hirnschall et al. 2014) and in patients with cataracts (Martínez-Roda et al. 2016b), significantly divergent results of forward light scatter have been obtained. Double-pass (DP) systems and the objective scatter index (OSI) (Artal et al. 2011) have been widely used to classify cataracts in clinical environments (Vilaseca et al. 2012). An increase in the OSI has been observed in eyes with keratoconus (Leonard et al. 2016), and significant correlations have been found between the OSI and the logMAR in patients after corneal transplantation (Kamiya et al. 2015). The OSI compares the integrated intensity contained in a ring between 0.20° and 0.33° (degrees), that is, between 12 and 20 min of arc, with the integrated intensity contained in the central area of the DP image within 1 min of arc. However, the presence of aberrations can affect the OSI (Miao et al. 2014). Ginis et al. (2012) recently presented an experimental system to reconstruct a wide-angle version of the point spread function (PSF) of the eye, where the reconstructed curve contains data up to 8° and may be used to quantify intraocular scattering. Due to its characteristics, the system is restricted to an area of 2 mm in exit pupil diameter and does not provide information on aberrations.

In this study, we propose a new parameter to quantify intraocular scattering based on the analysis of the information contained in the DP image at eccentricities between 0.59° and 2.35°, in order to minimize the impact of aberrations on the results. The region selected is hardly affected by aberrations

while containing the effects of intraocular scattering (van den Berg et al. 2009). Furthermore, the DP image used incorporates the overall effects of scattering within an exit pupil diameter of 4 mm. The parameter is computed in the frequency domain applied to the lowest part of the spectrum of the DP image, specifically the range comprised between 0 and 3 cycles per degree (cpd) of the ocular modulation transfer function (MTF).

## Methods

To analyse the performance of the parameter proposed in a clinical setting, we conducted a study in patients diagnosed with nuclear cataracts of different severity, and in a control group (CG) of subjects with healthy eyes. This prospective study was approved by the *Hospital Universitari Mútua de Terrassa* ethics committee and conformed to the tenets of the Declaration of Helsinki (Tokyo revision, 2004). The study included patients who were scheduled for cataract check-ups and a CG of volunteers from our university. All patients signed a consent form after the purpose of the study had been explained. Inclusion criteria were the diagnosis of nuclear cataracts, with refractive spherical equivalent from -6.00 to +6.00 dioptres (D) and astigmatism below 3.00 D. Exclusion criteria were the diagnosis of any other eye condition, presence of corneal opacities and history of ocular trauma or surgery.

Manifest refraction and corrected distance visual acuity (CDVA) were assessed under physiological pupil conditions. After pupil dilation with 0.2 ml of 1% tropicamide, a slit lamp examination was performed; the ophthalmologist determined the type and grade of cataract in terms of lens opacity [nuclear opacity 1, 2 and 3 (NO1, NO2 and NO3)] within the LOCS III classification system.

The protocol included measurement of forward intraocular scattering with the HD Analyzer instrument (Visiometrics S.L., Cerdanyola del Vallès, Barcelona, Spain) by means of the OSI (Artal et al. 2011) and with the DP experimental instrument described in section Experimental setup and image acquisition by means of the new Frequency Scatter Index ( $FSI_3$ ).

### Experimental set-up and image acquisition

We used an experimental DP instrument to acquire DP images as described

elsewhere (Artal et al. 2011). In this study, the diameter of the exit pupil was set to 4 mm for the whole procedure. Briefly, the instrument records the retinal image corresponding to a point-source object in the near-infrared, consisting of a laser diode (MC7800C-M-004S-7A10, wavelength 780 nm; Monocrom S.L., Vilanova i la Geltru, Spain) coupled to an optical fibre, after diffuse reflection on the ocular fundus and double pass through the ocular media. The experimental device used is shown in Fig. 1.

During measurements, collimated light from the laser source (LD) was transmitted by the linear polarizer LP1 before reaching the circular diaphragm AP1 of 2 mm in diameter that acted as entrance pupil. After being transmitted by the beam splitter BS2 and reflected by mirror M1, the light interacted with the Badal system formed by two identical lenses (L1 and L2) of 150 mm in focal length. This configuration was used to correct the spherical refractive error of patients between -6.00 and +6.00 D, modifying the optical distance between the lenses with the remote-controlled step motor that moved forward or backward mirrors M2 and M3. After lens L2, the light was reflected by mirror M4 before reaching the pupil plane of the eye and focusing the light onto the retina of the patient.

After interacting with the ocular fundus, the reflected light followed an optical path identical to the first pass until it reached the beam splitter BS2, which reflected the light coming from the eye towards the exit pupil of 4 mm in diameter formed by diaphragm AP2. The light was then filtered by the linear polarizer LP2, which removed corneal reflections in combination with the crossed polarizer LP1 located within the first-pass optical path. Finally, lens L3 of 50 mm in focal length focused the DP spot on the sensor of the imaging device CCD1 (Electron Multiplying CCD Luca<sup>EM</sup> R, Andor Technology<sup>TM</sup>, Belfast, UK). This 14-bit-depth cooled camera recorded DP images with a pixel resolution of 8 μm × 8 μm (0.55 min of arc) using a sensor of 8 mm × 8 mm, providing single photon detection sensitivity at all eccentricities. This method ensures the measurement of all light reflected back from the retina, which contains the effects of forward light scatter, light diffusion in the choroid and aberrations.

Additionally, a rotating motor was mounted on mirror M2. The vibration provided by the motor allowed M2 to act as a scanning mirror to obtain images with reduced speckle (Hofer et al. 2001; Sanabria et al. 2014). During measurements, the pupil position in the image provided by camera CCD2 (UI-1226LE-M; IDS Imaging Development Systems GmbH, Obersulm, Germany) monitored the alignment between the optical axis of the system and the eye. The imaging device processed the light at 900 nm from the light emitting diodes placed in front of the eye after imaging the pupil plane with lenses L2 and L5, mirrors M4 and M5, and dichroic mirror. The LD, motor SM, and cameras CCD1 and CCD2 were controlled remotely using the personal computer through a customized program in JAVA (Oracle, Java SE and NetBeans, version 8.0.2; Redwood City, CA, USA, 2015) developed in the open-source platform Micro-Manager (Edelstein et al. 2010). Once acquired, the DP images were processed offline using the open-source software IMAGEJ (Schneider et al. 2012).

The light reaching the eye was measured with a radiometer IL 1700 (International Light Technologies, Peabody, MA, USA). The irradiance for the 780 nm LD measured at the corneal plane was of 0.48 W/m<sup>2</sup>, a value considerably lower than the maximum permissible exposure of 14.45 W/m<sup>2</sup> defined in the corresponding standards (International Electrotechnical Commission. Safety of laser products – part 1: Equipment classification and requirements. IEC 60825-1:2014, Edition 3, May 2014).

The Badal system of the instrument automatically corrected the patients' spherical refraction, while astigmatism was corrected with an external cylindrical lens. A set of six consecutive DP images, each obtained with an exposure time of 200 ms, was recorded, and the average of the images was calculated. Another image was acquired with the eye removed from the system and subtracted from the first one to obtain the image used for the analysis.

### Intraocular scattering assessment

#### Preliminary assumptions

Double-pass (DP) images contain the overall effects of both aberrations and scattering (Díaz-Santana & Dainty 2001; Díaz-Doutón et al. 2006).

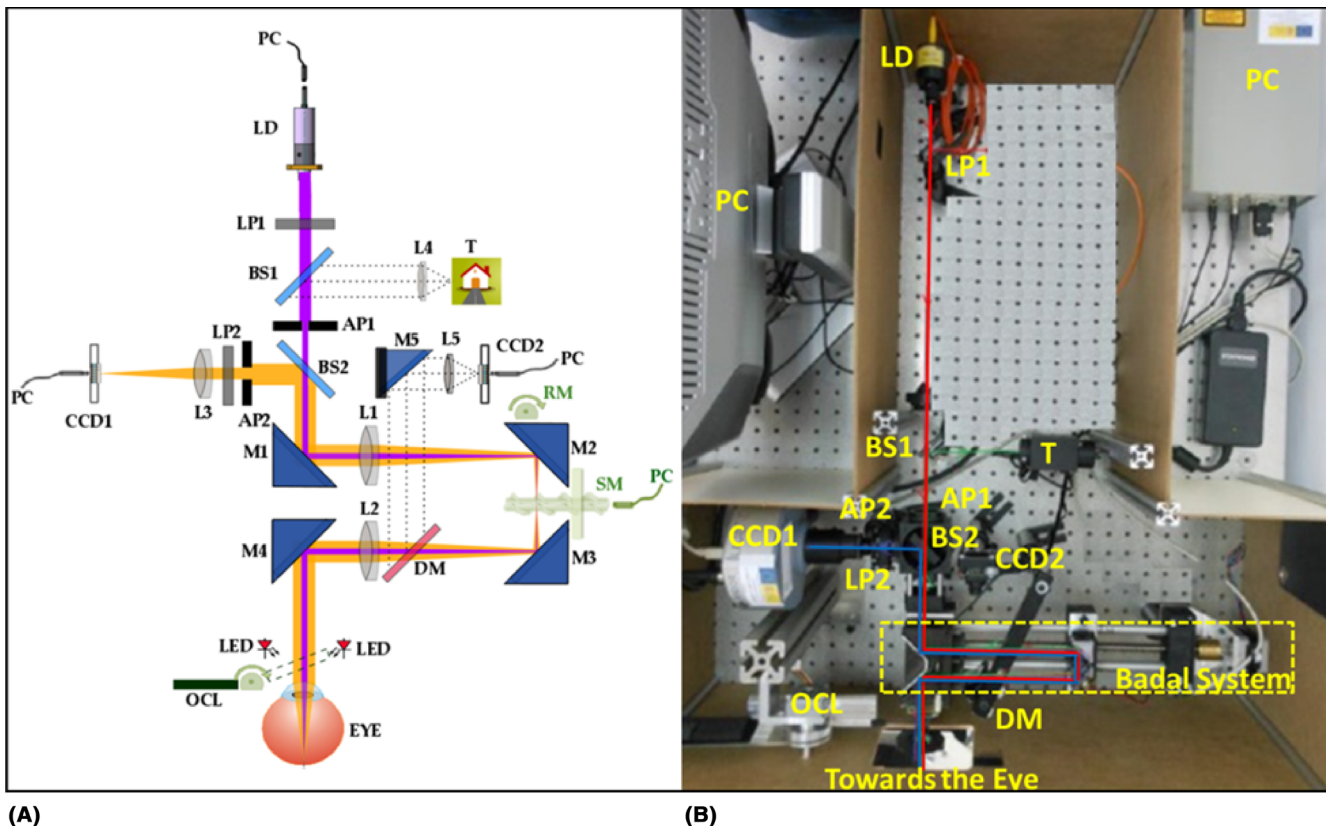


**Fig. 1.** Layout (A) and picture (B) of the double-pass set-up. AP = pupil, BS = beam splitters, CCD = Charge-coupled device, DM = dichroic mirror, L = lens, LD = laser diode, LP = linear polarizer, M = mirror, OCL = occluder, PC = personal computer, RM = rotating motor, SM = step motor, T = test. In purple, the optical path of the first-pass, and in orange, the optical path of the second-pass.

However, it seems reasonable to consider that the information about aberrations and scattering is spatially distributed: while the effects of aberrations are preponderant in the area closest to the peak of maximum intensity, the ones of scattering predominate in more eccentric areas.

To implement the  $FSI_3$ , two MTF curves are obtained after applying a Fourier transform to two cropped versions of the DP image with squared regions of interest of extensions  $r_1$  and  $r_2$ , with  $r_1 < r_2$ , and a common central position defined by the peak with maximum intensity of the image (Fig. 2). In the region defined by  $r_1$ , the effects of aberrations mask the ones of scattering. On the contrary, the effects of aberrations are negligible compared to the ones of scattering in the borders of the region defined by  $r_2$ . In this work, we analyse MTF curves obtained from regions with  $r_1 = 0.59^\circ$  ( $128 \times 128$  pixels) and  $r_2 = 2.35^\circ$  ( $512 \times 512$  pixels) of the DP image to obtain the  $FSI_3$ .

To evaluate the effects of intraocular scattering in the two proposed regions

of interest (ROI), we used the commercially available diffusers Black Pro-Mist (BPM) 1 and 2 (Tiffen, Hauppauge, NY, USA), widely employed to simulate incipient and moderate cataracts, respectively (De Wit et al. 2006). Each diffuser was placed in front of an artificial eye consisting of a lens of 50 mm in focal length and a cardboard working as a retina, as well as in front of two human eyes from two volunteers aged 23 and 54 years. The graphs on the left of Fig. 3 show the normalized radial average of the MTF curves obtained with the ROI of size  $r_1$  ( $MTF_{DP[0.59^\circ]}$ ). As can be seen, the diffuser filters barely affect the MTFs obtained. The graphs on the right show the MTF curves obtained with the ROI of size  $r_2$  ( $MTF_{DP[2.35^\circ]}$ ), where, by contrast, the effect of the diffuser filters is noticeable.

Some authors have presented models where the effects of aberrations and scattering are included in the MTF of the eye in a multiplicative form (Rodríguez et al. 2007). Assuming this as true, and considering that  $MTF_{DP[0.59^\circ]}$  is basically affected by aberrations

and that  $MTF_{DP[2.35^\circ]}$  is affected by both aberrations and diffusion, we can use the ratio between the MTFs obtained from the two ROIs ( $MTF_{F[r_2-r_1]}$ ) to estimate the effect of diffusion in the ocular media as follows:

$$\frac{MTF_{DP[r_2]}(v)}{MTF_{DP[r_1]}(v)} \propto \sim MTF_{F[r_2-r_1]}(v).$$

The ratios  $MTF_{F[r_2-r_1]}$  for the artificial and the two human eyes under the presence of the different diffusers considering ROIs with sizes  $r_1 = 0.59^\circ$  and  $r_2 = 2.35^\circ$  are shown in Fig. 4. As observed, in all three cases a similar pattern is observed, that is, an abrupt drop at lower frequencies and a stable behaviour beyond approximately 3 cpd. The former is related to the amount of induced intraocular scattering, and as expected, it was higher for the older eye (Rozema et al. 2010; Martínez-Roda et al. 2016a).

#### Definition of the Frequency Scatter Index ( $FSI_3$ )

The aforementioned results verify the assumption that information on

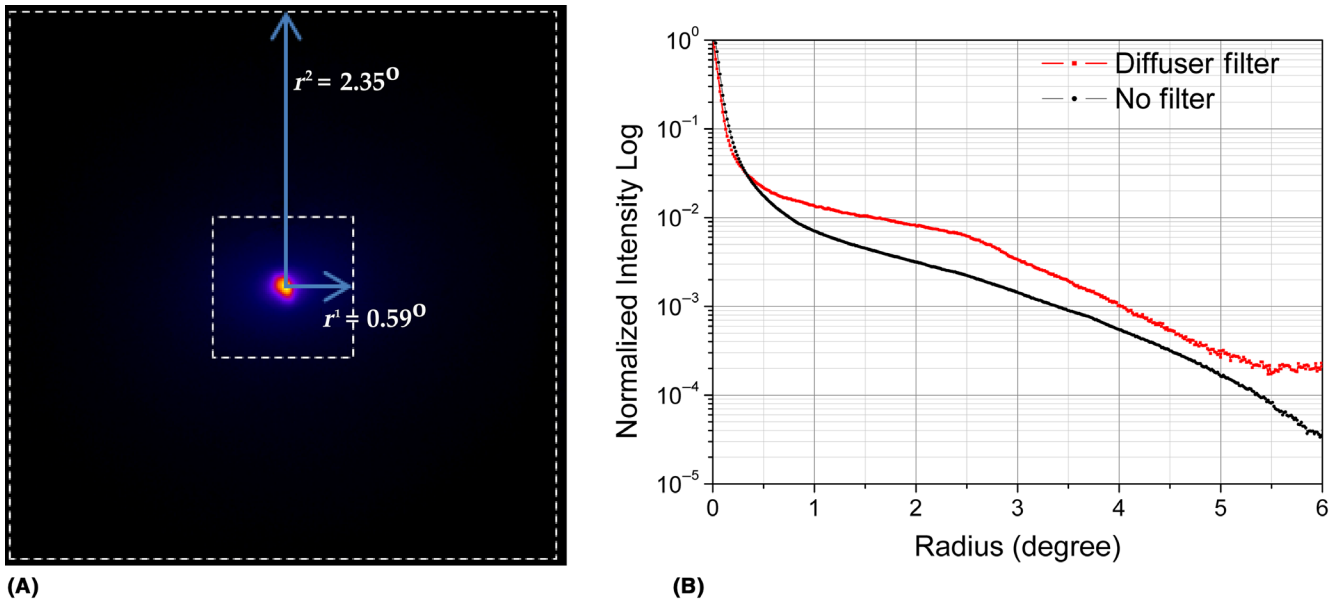


**Fig. 2.** Pseudocolour double-pass (DP) image (A): marked by dashed white lines with regions of interest of  $128 \times 128$  pixels ( $r_1 = 0.59^\circ$ ) and  $512 \times 512$  pixels ( $r_2 = 2.35^\circ$ ). Radial average profile in logarithmic scale of the DP image (B): corresponding to the image on the left (black) and with a diffuser filter in front of the same eye (red); dashed lines indicate the position of  $r_1$  and  $r_2$ .

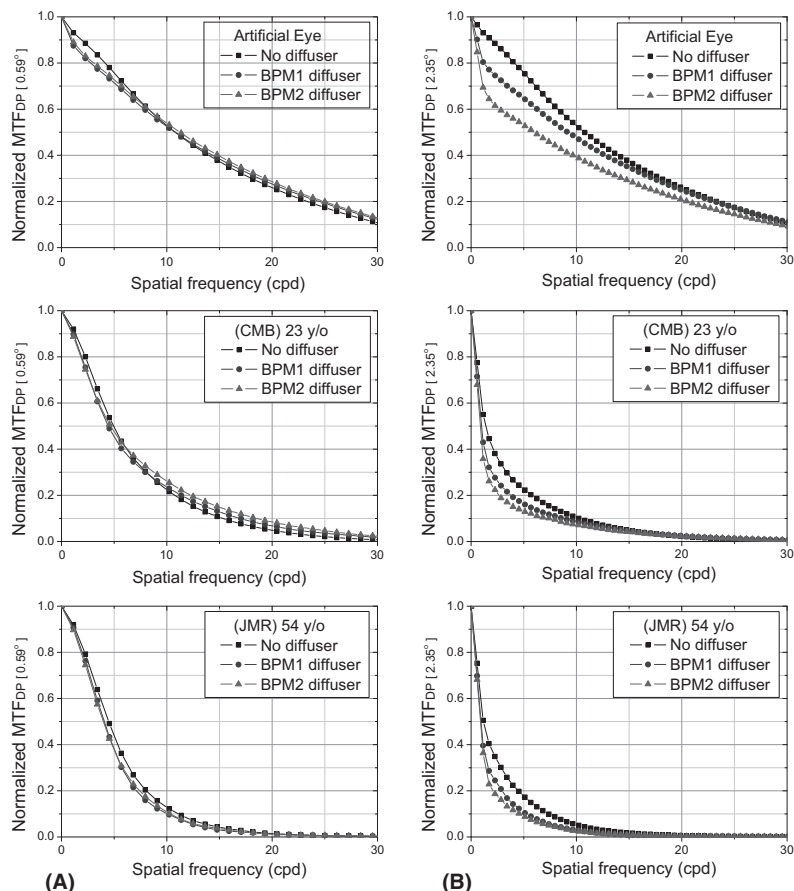


**Fig. 3.** Normalized mean radial profile of the MTF<sub>DP</sub> without diffuser (squares) and with diffuser BPM1 (circles) and BPM2 (triangles), regions of interest with sizes  $r_1 = 0.59^\circ$  (A), and  $r_2 = 2.35^\circ$  (B), for the artificial eye (top) and the two eyes of volunteers aged 23 (middle) and 54 (bottom). BPM = Black Pro-Mist.

intraocular scattering is contained mainly at lower spatial frequencies. Accordingly, a novel parameter to quantify intraocular scattering ( $FSI_3$ ) is proposed as follows:

$$FSI_3 = \frac{n}{\sum_{v=0}^{n(v<3\text{cpd})} MTF_{F[r_2-r_1]}(v)} - 1$$

where subindex 3 indicates that only frequency values between 0 and 3 cpd of the MTF<sub>DP</sub> are included. Specifically, in our set-up  $n$  was set to 6, since these discrete numbers of frequencies were available in the interval considered – from 0 to 3 cpd. In accordance with the formula,  $FSI_3$  values over 1 are obtained in the presence of intraocular scattering. In order to establish a parameter with a null value in the absence of intraocular scattering, 1 is finally subtracted from the equation. Moreover, the parameter depends on the size of the selected ROIs. In our case, the weight of the information contained is evaluated up to an angle of  $2.35^\circ$  compared to that of  $0.59^\circ$ .

**Impact of intraocular scatter on  $FSI_3$**   
To corroborate its correct performance, the proposed parameter was used to assess intraocular scattering in the artificial and human eyes of volunteers aged 23 and 54 years with and without diffusers BPM1 and BPM2. Five repeated measurements were

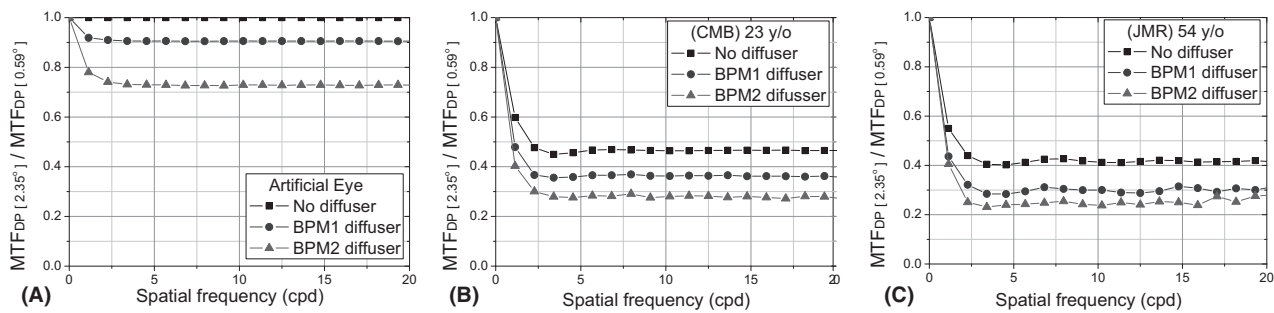


**Fig. 4.**  $MTF_{FRP[2.35^\circ]}(v)$  without diffuser (squares) and with diffuser BPM1 (circles) and BPM2 (triangles) for the artificial eye (A) and the two eyes of volunteers aged 23 (B) and 54 (C) years. BPM = Black Pro-Mist.

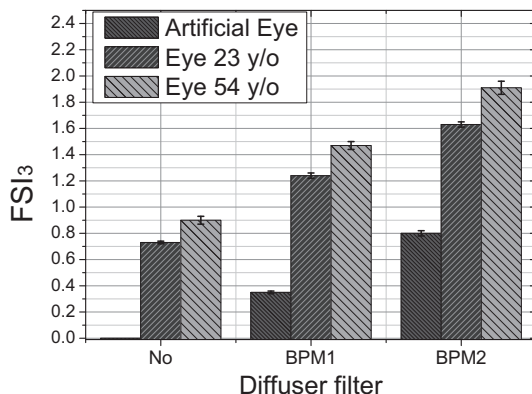


**Fig. 5.** Bar chart plot with the mean and the standard deviation values of five repeated measurements of the Frequency Scatter Index parameter for the artificial and the two eyes of volunteers aged 23 and 54 years without diffuser (No) and with diffusers Black Pro-Mist 1 and 2.

obtained for each eye. Figure 5 shows the mean and the standard deviation of this computation. The  $FSI_3$  increases for all eyes in correlation with the level of scattering. As expected, the older eye shows higher  $FSI_3$  values, whereas the lowest values correspond to the artificial eye.

The fact that the parameter does not get a 0 value for the 23-year-old subject without scattering may be attributable to lateral diffusion in the layers of the retina or even in the choroid due to the wavelength used (Delori & Pflibsen 1989; Williams et al. 1994). Even so, the differences between the two individuals are small compared to the increase with diffuser filters.

#### Impact of defocus on $FSI_3$

The performance of the  $FSI_3$  under defocus was also studied as a preliminary validation. To this end, measurements from the two subjects aged 23 and 54 years were again obtained under different amounts of induced defocus, specifically between 0.00 and 2.50 D in steps of 0.50 D induced by

means of the Badal system available in the experimental set-up. The difference between values of  $FSI_3$  without defocus and values with a maximum defocus of 2.50 D were of 0.20 and 0.30 for the two subjects, respectively. Figure 6 shows the  $FSI_3$  values for 0.00 D and other defocus conditions, proving that  $FSI_3$  values increased minimally with defocus, which demonstrates the robustness of this parameter in the presence of this low-order aberration. In contrast, the OSI increased significantly from 1.00 D defocus, probably because the defocus causes a sharp decrease in the PSF peak. In this case, the maximum differences were 4.02 (in terms of OSI) at a 2.50 D defocus for both subjects.

The observed behaviour was already expected because the  $FSI_3$  includes the region of the DP image between  $0.59^\circ$  and  $2.35^\circ$ , much larger than the OSI region (from  $0.20^\circ$  to  $0.33^\circ$ ). The OSI region is very close to the central peak of the image and thus more affected by aberrations, whereas scattering dominates the

behaviour of the region used to calculate the  $FSI_3$ .

#### Statistical analysis

The Shapiro-Wilk test was used to evaluate the normal distribution of the  $FSI_3$ , OSI and CDVA. An independent sample t-test was used to compare the mean between the CG and the eyes with cataracts and between each LOC-SIII subgroup (NO1, NO2 and NO3). Since the OSI data did not meet the criteria for normal distribution, the Mann-Whitney U-test ( $z$ ) was used to compare the data between subgroups NO1, NO2 and NO3, and the Spearman rank correlation coefficient ( $\rho$ ) was calculated to assess the relationships between the  $FSI_3$ , the OSI and the CDVA. Chi-square tests were used to compare the proportion of sex and age within the groups. Descriptive data are shown as the mean  $\pm$  standard deviation (SD) for normally distributed variables and median and interquartile range for non-normally distributed variables. A value of  $p < 0.05$  was considered statistically significant.

## Results

Patient demographics are shown in Table 1. Nine control eyes of nine healthy observers and 19 eyes of 19 patients diagnosed exclusively with aged-related nuclear cataracts were finally included in the study. No statistically significant differences were noted between the CG and cataract group or among the LOC-SIII-grade subgroups (NO1, NO2 and NO3) regarding sex, right/left eye or manifest subjective refraction. There was a significant difference in terms of averaged age between the CG and the cataract group ( $p < 0.001$ );

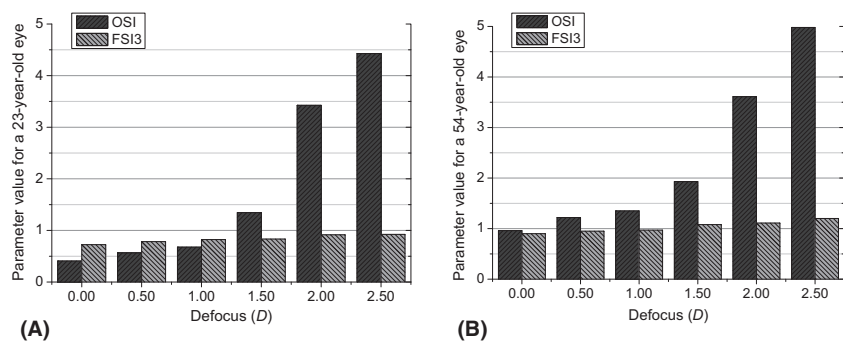


**Fig. 6.** Frequency Scatter Index (measured with the experimental set-up) and objective scatter index (measured with the commercial HDA instrument) at the best focus position and with induced defocus up to 2.50 D in 0.50 D steps: (A) volunteer aged 23 and (B) volunteer aged 54.

**Table 1.** Demographic of the control and cataract groups according to sex, eye, age and manifest subjective refraction (spherical equivalent).

Parameter	CG	Cataract group		
		Subgroups of LOCSIII grade	NO1	NO2
Sex (n)				
Male	5	4	6	2
Female	4	2	2	3
Eye (n)				
Right	4	4	3	2
Left	5	2	5	3
Age (years)				
Mean (SD)	55 (3)	71 (8)	71 (6)	73 (6)
Range (min max)	50 58	56 80	60 77	66 80
Spherical equivalent (D)				
Mean (SD)	-0.38 (1.61)	+0.75 (1.30)	-0.77 (2.85)	+1.10 (2.59)
Range (min max)	-3.50 +1.50	-1.38 +2.63	-5.13 +2.37	-2.50 +4.50

CG = control group, NO = nuclear opacity, SD = standard deviation.

**Table 2.** FSI<sub>3</sub>, OSI and CDVA values of the control and cataract groups.

Parameter	CG	Cataract group		
		Subgroups of LOCSIII grade	NO1	NO2
FSI <sub>3</sub>				
Mean (SD)	1.18 (0.20)	1.30 (0.12)	1.62 (0.21)	1.85 (0.21)
OSI				
Median (IQR)	1.30 (0.24)	1.63 (0.47)	3.26 (0.78)	4.06 (1.83)
CDVA (LogMAR)				
Median (IQR)	0.00 (0.02)	0.26 (0.57)	0.35 (0.19)	0.40 (0.29)

CDVA = corrected distance visual acuity, CG = control group, FSI<sub>3</sub> = Frequency Scatter Index, IQR = interquartile range, NO = nuclear opacity, OSI = objective scatter index, SD = standard deviation.

no age difference existed among the LOCSIII subgroups ( $p > 0.05$ ).

The FSI<sub>3</sub> was significantly higher ( $p = 0.001$ , *t*-test) in the cataract group than in the CG. Table 2 shows how the averaged FSI<sub>3</sub> increases with the LOCSIII grade. We found statistically significant differences between subgroups

NO1 and NO2 ( $p = 0.005$ ), but not between NO2 and NO3 ( $p = 0.050$ ). The OSI was also significantly higher in the cataract group compared to the CG ( $p < 0.001$ , Mann–Whitney *U*-test), and significant differences were found between subgroups NO1 and NO2 ( $p = 0.002$ ) and NO2 and NO3

( $p = 0.003$ ). The CDVA was also significantly higher in the cataract group than in the CG ( $p < 0.001$ ), but the differences between NO1 and NO2 and between NO2 and NO3 were not statistically significant ( $p > 0.05$ ).

In addition, we found very strong correlations between the FSI<sub>3</sub> and the OSI ( $\rho = 0.861$ ,  $p < 0.001$ ) and between the OSI and the CDVA ( $\rho = 0.672$ ,  $p < 0.001$ ), but moderate between FSI<sub>3</sub> and CDVA ( $\rho = 0.508$ ,  $p = 0.006$ ; Fig. 7). A similar correlation was found between the FSI<sub>3</sub> and the OSI when the CG ( $\rho = 0.733$ ,  $p = 0.025$ ) and the cataract group ( $\rho = 0.773$ ,  $p < 0.001$ ) were separately analysed.

Finally, the scatterplot for the individual FSI<sub>3</sub> and OSI values with different scales for each parameter is shown in Fig. 8. Interestingly, FSI<sub>3</sub> and OSI share approximately 70% of information about intraocular scattering.

## Discussion

The analysis of intensity distribution in the DP image has been widely used to obtain information about the contribution of aberrations and intraocular scattering on the retinal image. The proposed FSI<sub>3</sub> quantifies scattering from a wide region of the DP image which subtends an angle of 2.35° and applies only to low spatial frequencies, that is, below 3 cpd. The results show that the new parameter is very sensitive to the presence of scattering caused by commercial diffusers. Furthermore, preliminary validations demonstrate that only the measurement for the artificial eye provides a null FSI<sub>3</sub> value, whereas human eyes with cataracts show a scattering value comparable to that induced with the BPM1 diffuser.

When computing the FSI<sub>3</sub> parameter, the information where the effects of aberrations are dominant is filtered to minimize its impact. In consequence, the defocus values up to 2.50 D in the DP image have little impact on the FSI<sub>3</sub> when measuring scattering, particularly in comparison with the widely used OSI. Specifically, in the case of the OSI, an induced defocus of the DP image above 1.00 D results in a considerable overestimation of scattering, according to this and previous studies (Artal et al. 2011).

With regard to the results of patients with cataracts, forward and backward light scatter measurements cannot be

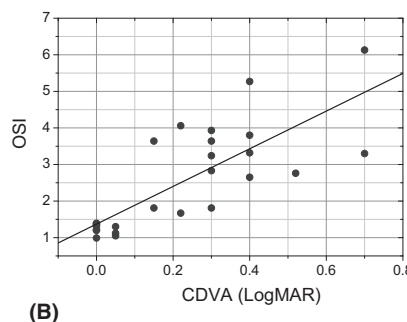
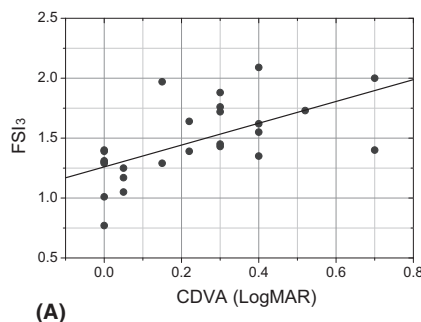


**Fig. 7.** Scatterplot with the individual values of corrected distance visual acuity (x-axis) and Frequency Scatter Index (A) ( $r^2 = 0.258$ ) and objective scatter index (B) ( $r^2 = 0.310$ ) (y-axis).

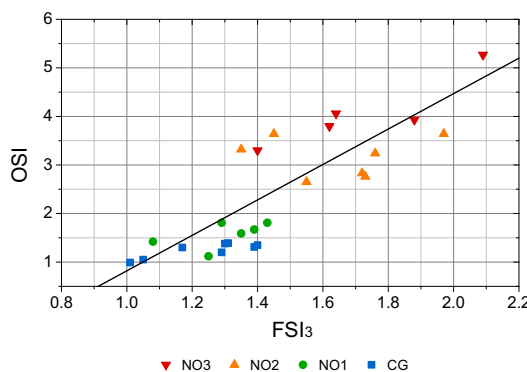


**Fig. 8.** Scatterplot with the individual values of Frequency Scatter Index (x-axis) and objective scatter index (y-axis) ( $r^2 = 0.698$ ). Markers in colours by subgroups of LOCSIII grade (NO1, NO2 and NO3) and control group (CG).

used interchangeably. Slit lamp grading is based on backward light scatter, whereas the FSI<sub>3</sub> measures forward scattering, although a strong correlation exists between the FSI<sub>3</sub> and NO. The better correlation between NO and OSI is probably due to OSI scattering overestimates caused by the presence of higher-order aberrations in eyes with mature cataracts (Rocha et al. 2007; Lee et al. 2008). On the other hand, FSI<sub>3</sub> and OSI share approximately 70% of scatter in our sample of patients with cataracts (Fig. 8). At this point, it should be borne in mind that in this study an experimental device has been used, whose configuration and components slightly differ from commercially available DP instruments. Especially the 14-bit-depth cooled camera allows obtaining information with very low noise level. The suitability of devices with different configurations or characteristics to quantify forward scattering with the new parameter has not been subject of this study. Another limitation of this study is the limited number of patients. Therefore, it would

be also necessary to expand it to determine the FSI<sub>3</sub> values in healthy patients and for the different degrees of severity of cataracts.

In conclusion, this study presents a novel parameter for measuring intraocular scattering computed from DP images in the frequency domain with a minimal impact of aberrations. The main objective of the FSI<sub>3</sub> would be to obtain measurements less dependent on patients' refractive error compensation and higher-order aberrations. The parameter is sensitive to scattering induced by diffusers and caused by cataracts. Furthermore, it discriminates the information on scatter and aberrations contained in the DP image more effectively than the OSI. The parameter FSI<sub>3</sub> evaluates the information contained in an area that subtends from 0.59° to 2.35° of the DP image which includes the intraocular scattering and the scatter that occurs in the inner layers of the retina. The use of a different wavelength with less penetration would allow diminishing the influence of this scatter. Even so, the results indicate that

this has a much lower value than that caused by intraocular diffusion in patients with cataract. In addition, the variability between healthy individuals is also small compared to the presence of cataracts, although it should be studied in a greater number of individuals.

Additionally, the integration of these two objective parameters results in a greater understanding of these visual phenomena with regard to different ocular conditions in clinical and research settings (Jinabhai et al. 2012; Kamiya et al. 2015; Leonard et al. 2016). Further studies will analyse a larger number of patients with different patterns of scatter, especially posterior subcapsular and cortical cataracts, as well as in different corneal pathologies that cause scattering and age-matched controls. Furthermore, the suitability of the proposed methodology using eight-bit-depth cameras, which are nowadays included in commercially available DP instruments, will be also studied. Regardless the fact that we used six discrete frequencies for the computation of the FSI<sub>3</sub> as this was the number of values available within the frequency range considered in our system, the methodology is still valid for any other frequency sampling between 0 and 3 cpd available in any other set-up.

## References

- Artal P, Benito A, Pérez GM, Alcón E, De Casas A, Pujol J & Marín JM (2011): An objective scatter index based on double-pass retinal images of a point source to classify cataracts. *PLoS ONE* **6**: e16823.
- van den Berg TJTP, Franssen L & Coppens JE (2009): Straylight in the human eye: testing objectivity and optical character of the psychophysical measurement. *Ophthalmic Physiol Opt* **29**: 345–350.
- De Wit GC, Franssen L, Coppens JE & Van Den Berg TJTP (2006): Simulating the straylight effects of cataracts. *J Cataract Refract Surg* **32**: 294–300.
- Delori FC & Pflibsen KP (1989): Spectral reflectance of the human ocular fundus. *Appl Opt* **28**: 1061–1077.
- Díaz-Doutón F, Benito A, Pujol J, Arjona M, Güell JL & Artal P (2006): Comparison of the retinal image quality with a Hartmann-Shack wavefront sensor and a double-pass instrument. *Invest Ophthalmol Vis Sci* **47**: 1710–1716.
- Díaz-Santana L & Dainty JC (2001): Effects of retinal scattering in the ocular double-pass process. *J Opt Soc Am A* **18**: 1437–1444.
- Edelstein A, Amodaj N, Hoover K, Vale R & Stuurman N (2010): Computer control of

- microscopes using μManager. *Curr Protoc Mol Biol Chapter 14*: Unit14.20.
- Franssen L, Coppens J & van den Berg TJ (2006): Compensation comparison method for assessment of retinal straylight. *Ophthalmol Vis Sci* **47**: 768–776.
- Ginis H, Perez GM, Bueno JM & Artal P (2012): The wide-angle point spread function of the human eye reconstructed by a new optical method. *J Vis* **12**: 20.
- Hirnschall N, Crnej A, Gangwani V & Findl O (2014): Comparison of methods to quantify posterior capsule opacification using forward and backward light scattering. *J Cataract Refract Surg* **40**: 728–735.
- Hofer H, Artal P, Singer B, Aragón JL & Williams DR (2001): Dynamics of the eye's wave aberration. *J Opt Soc Am A* **18**: 497.
- Jinabhai A, O'Donnell C, Radhakrishnan H & Nourrit V (2012): Forward light scatter and contrast sensitivity in keratoconic patients. *Cont Lens Anterior Eye* **35**: 22–27.
- Kamiya K, Asato H, Shimizu K, Kobashi H & Igarashi A (2015): Effect of intraocular forward scattering and corneal higher-order aberrations on visual acuity after Descemet's stripping automated endothelial keratoplasty. *PLoS ONE* **10**: e0131110.
- Lee J, Kim MJ & Tchah H (2008): Higher-order aberrations induced by nuclear cataract. *J Cataract Refract Surg* **34**: 2104–2109.
- Leonard AP, Gardner SD, Rocha KM, Zeldin ER, Tremblay DM & Waring GO (2016): Double-pass retina point imaging for the evaluation of optical light scatter, retinal image quality, and staging of keratoconus. *J Refract Surg* **32**: 760–765.
- Martínez-Roda JA, Vilaseca M, Ondategui JC, Aguirre M & Pujol J (2016a): Effects of aging on optical quality and visual function. *Clin Exp Optom* **99**: 518–525.
- Martínez-Roda JA, Vilaseca M, Ondategui JC, Almudí L, Asaad M, Mateos-Pena L, Arjona M & Pujol J (2016b): Double-pass technique and compensation-comparison method in eyes with cataract. *J Cataract Refract Surg* **42**: 1461–1469.
- Miao H, Tian M, He L, Zhao J, Mo X & Zhou X (2014): Objective optical quality and intraocular scattering in myopic adults. *Invest Ophthalmol Vis Sci* **55**: 5582–5587.
- Rocha KM, Nosé W, Bottós K, Bottós J, Morimoto L & Soriano E (2007): Higher-order aberrations of age-related cataract. *J Cataract Refract Surg* **33**: 1442–1446.
- Rodríguez P, Navarro R, Rodríguez P & Navarro R (2007): Double-pass versus aberrometric modulation transfer function in green light. *J Biomed Opt* **12**: 044018.
- Rozema JJ, Van den Berg TJTP & Tassignon M-J (2010): Retinal straylight as a function of age and ocular biometry in healthy eyes. *Invest Ophthalmol Vis Sci* **51**: 2795–2799.
- Sanabria F, Arévalo MA, Díaz-Doutón F, García-Guerra CE & Ramo JP (2014): Technical improvements applied to a double-pass setup for performance and cost optimization. *Opt Eng* **53**: 061710.
- Schneider CA, Rasband WS & Eliceiri KW (2012): NIH Image to ImageJ: 25 years of image analysis. *Nat Methods* **9**: 671–675.
- Vilaseca M, Romero MJ, Arjona M et al. (2012): Grading nuclear, cortical and posterior subcapsular cataracts using an objective scatter index measured with a double-pass system. *Br J Ophthalmol* **96**: 1204–1210.
- Westheimer G & Liang J (1994): Evaluating diffusion of light in the eye by objective means. *Invest Ophthalmol Vis Sci* **35**: 2652–2657.
- Williams DR, Brainard DH, McMahon MJ & Navarro R (1994): Double-pass and interferometric measures of the optical quality of the eye. *J Opt Soc Am A* **11**: 3123.

Received on February 7th, 2019.

Accepted on March 28th, 2019.

*Correspondence:*

Joan A. Martínez-Roda, PhD  
Centre for Sensors, Instruments and Systems Development (CD6)  
Universitat Politècnica de Catalunya (UPC)  
Rambla Sant Nebridi 10  
08222 Terrassa  
Barcelona, Spain  
Tel: +34 93 739 8908  
Fax: +34 93 739 89 23  
Email: juanantonio.martinez@upc.edu

The research leading to these results has received funding from the Spanish Ministry for Science and Innovation (MICINN; DPI2011-30090-C02-01), from the European Union's Horizon 2020 research and innovation programme under the Marie Skłodowska-Curie grant agreement No. 712949 (TECNIOspring PLUS) and from the Agency for Business Competitiveness of the Government of Catalonia.